International Journal of Minerals, Metallurgy and Materials
Volume 21, Number 10, October 2014, Page 1019
DOI: 10.1007/s12613-014-1003-9

Dielectric, piezoelectric, and ferroelectric properties of lanthanum-modified PZTFN ceramics

Arvind Kumar[1)] *and S. K. Mishra*[2)]

1) Research and Technology Development Centre, Sharda University, Greater Noida 201306, India
2) Dr. Harisingh Gour University, Sagar (M.P.), Sagar 470003, India

(Received: 3 February 2014; revised: 16 April 2014; accepted: 24 April 2014)

Abstract: Specimens of $Pb_{1-1.5x}La_x(Zr_{0.53}Ti_{0.47})_{1-y-z}Fe_yNb_zO_3$ (x = 0, 0.004, 0.008, 0.012, and 0.016, $y = z$ = 0.01) (PZTFN) ceramics were synthesized by a semi-wet route. In the present study, the effect of La doping was investigated on the structural, microstructural, dielectric, piezoelectric, and ferroelectric properties of the ceramics. The results show that, the tetragonal (space group *P*4*mm*) and rhombohedral (space group *R*3*c*) phases are observed to coexist in the sample at x = 0.012. Microstructural investigations of all the samples reveal that La doping inhibits grain growth. Doping of La into PZTFN improves the dielectric, ferroelectric, and piezoelectric properties of the ceramics. The hysteresis loops of all specimens exhibit nonlinear behavior. The dielectric, piezoelectric and ferroelectric properties show a maximum response at $x \geq 0.012$, which corresponds to the morphotropic phase boundary (MPB).

Keywords: ceramics; lanthanum; doping; dielectric properties; piezoelectricity; ferroelectricity; Rietveld refinement; hysteresis loops

1. Introduction

$Pb(Zr_{1-x}Ti_x)O_3$ (PZT) materials have been reported over the past decades to have the wide applications in science and technology [1–2]. PZT is a solid solution of lead titanate ($PbTiO_3$) and lead zirconate ($PbZrO_3$). It exhibits excellent piezoelectric properties for $x \approx 0.48$, which corresponds to a morphotropic phase boundary (MPB) at which the tetragonal and rhombohedral phases coexist [3–4]. Various researchers have investigated the properties of compositionally modified PZT ceramics for technological applications. The pure PZT ceramic modified with zirconium (Zr), strontium (Sr), and yttrium (Y) exhibits good dielectric and piezoelectric responses [5]. Similarly, PZT modified with lanthanum (La), niobium (Nb), and iron (Fe) exhibits the improved piezoelectric properties with low dielectric loss [6–7]. Ramam and Lopez [8] reported that the incorporation of barium (Ba) into PZT enhanced the room-temperature dielectric constant significantly. Bochenek [9] reported that doping of Nb into barium-substituted PZT ceramics resulted in the high dielectric constant, low dielectric loss, and high residual polarization.

Singh and Chatterjee [10] reported that La rich $(1-x)(BF_{0.50}–LF_{0.50})–x(PT)$ (BLF-PT) (x = 0.34, 0.40, 0.50, or 0.60) ceramics exhibited MPB near x = 40:60 with the maximum enhancement of dielectric, ferroelectric, and magnetic properties. Brajesh *et al.* [11] reported that the $[Pb_{0.94}Sr_{0.06}][(Mn_{1/3}Sb_{2/3})_{0.05}(Zr_{0.53}Ti_{0.47})_{0.95}]O_3$ ceramic exhibited the excellent responses of coupling factor (k_p), piezoelectric coefficient (d_{33}), and quality factor (Q_m). The $Pb_{1-x}Sr_x[(Zr_{0.52}Ti_{0.48})_{0.95}(Mn_{1/3}Nb_{2/3})_{0.05}]O_3$ ceramic system exhibited the maximum dielectric and piezoelectric responses at the composition of x = 0.050, which corresponds to the MPB [12].

Ryu *et al.* [13] investigated the effect of heating rate on the properties of pure and niobium-pentoxide (Nb_2O_5)-modified PZT. The densification behavior of pure PZT improved significantly at a higher heating rate, and it also influenced the piezoelectric properties of the pure PZT ceramic. However, in the case of the Nb_2O_5-modified PZT ceramic, the densification behavior and piezoelectric properties were not substantially affected by the heating rate. Fe doping in $Pb_{0.92}[La_{1-z}Fe_z]_{0.08}[Zr_{0.60}Ti_{0.40}]_{0.98}O_3$ (z = 0, 0.3, 0.6,

Corresponding author: S.K. Mishra E-mail: dr.sunilkmishra@gmail.com

0.9, and 1) (PLFZT) ceramics resulted in the diffuse phase transition, relaxor behavior, low dielectric constant, and high transition temperature [14]. Chu *et al.* [15] reported that doping of 5.5mol% of Nb into PZT increased its dielectric constant and electromechanical coupling coefficient. The $(1-x)(Fe_{1/2}Nb_{1/2})O_3$–$xPbTiO_3$ ($0.05 \leq x \leq 0.08$) ceramic system includes the tetragonal and monoclinic phases with space groups *P*4*mm* and *Cm*, respectively, near the morphotropic phase boundary [16]. Kahoul *et al.* [17] reported the $Pb_{1-x}Sm_x[(Zr_y,Ti_{1-y})_{0.98}(Fe_{1/2}Nb_{1/2})_{0.02}]O_3$ ceramics over the range of y = 0.47–0.57 and claimed that the MPB lay between y = 0.51 and 0.55. Prasatkhetragarn [18] reported that the $0.9Pb(Zr_{1/2}Ti_{1/2})O_3$–$0.1Pb(Fe_{1/3}Nb_{2/3})O_3$ ceramics synthesized by a solid-state mixed oxide technique exhibited two phase transitions: one corresponds to a transition from a rhombohedral phase to a tetragonal ferroelectric phase, and other corresponds to a tetragonal-to-cubic transition. The doping of Fe_2O_3 into the $Pb_{0.9}(La_{1-z}Fe_z)_{0.1}(Zr_{0.65}Ti_{0.35})_{0.975}O_3$ (PLFZT) (z = 0, 0.3, 0.5 and 0.7) ceramic resulted in an increase in the transition temperature and dielectric properties [19]. Shukla *et al.* [20] reported that PLZT ceramics exhibited a diffuse phase transition with increasing La content in PZT. PZT doped with acceptor ions, such as Fe (at the B-site), creates oxygen vacancies in the lattice. However, PZT doped with donor ions, such as La (at the A-site) and Nb (at the B-site), results in vacancies in the A-site known as lead vacancies [21]. Lead vacancies reduce the stress level in the crystalline lattice and allow internal movements in the lattice. Therefore, these effects increase the piezoelectric performance.

In the present study, the complex doping of two or more elements was expected to improve the properties, compared to those of single-element donor- or acceptor-doped PZT. $Pb_{1-1.5x}La_x(Zr_{0.53}Ti_{0.47})_{1-y-z}Fe_yNb_zO_3$ (PLZTFN) ceramics were formed by La doping at the A-sites and the multiple (Fe and Nb) ions doping at the B-sites of PZT ceramics. The dielectric and piezoelectric properties of PLZTFN ceramics were investigated with x = 0, 0.004, 0.008, 0.012, and 0.016, and $y = z$ = 0.01. The various compositions were prepared by a semi-wet route [22]. The findings related to the microstructure as well as the piezoelectric, ferroelectric, and dielectric behavior of PLZTFN ceramics were reported.

2. Experimental

La-modified PZTFN ceramics with x = 0, 0.004, 0.008, 0.012, and 0.016 were prepared by a semi-wet route. High-purity AR-grade $PbCO_3$ (99.9%), La_2O_3 (99.0%), $(Zr_{0.53}Ti_{0.47})O_2$ (99.0%), Fe_2CO_3 (99.0%), and Nb_2O_5 (99.0%) materials (Merck) were used in the present work. The precursor powders for the required compositions were thoroughly mixed in a ball mill for 7 h in the presence of acetone as a mixing medium. The powders were dried in a dust-free atmosphere and then calcined at 800°C for 4 h. The calcined powders were ball milled again to break the agglomerates. Powders obtained after ball milling were compacted into circular discs at a load of 6 kN. The pellets were sintered in a crucible at 1100°C for 3 h in the presence of $PbZrO_3$ powders to prevent PbO loss during the high-temperature sintering. The density of sintered samples was measured using Archimedes' principle. Electrodes were painted onto the sintered pellets using high-purity silver paste, and the pellets were fired at 500°C for 1 h. The samples were poled in a silicon oil bath at 120°C for 1 h under a static DC electrical field of 3.5 kV/mm.

Powder X-ray diffraction (XRD) patterns were recorded using a Rigaku X-ray diffractometer equipped with a Cu K_α radiation source. The XRD patterns of all specimens were recorded at a scan rate of 1º/mim over the 2θ range of 20º–70°. Microstructures of all specimens were studied using field-emission scanning electron microscopy (FE-SEM, Quanta 200 FEG). The ceramic surfaces were coated with gold for the FE-SEM studies. The dielectric constant (ε_r) and tangent loss ($\tan\delta$) of the ceramic specimens were studied as a function of temperature using a HIOKI-LCR (model 3532-50) meter in a PID-controlled heating chamber. A polarization-electrical field (P–E) hysteresis loop tracer (Marine India) based on a modified Sawyer-Tower circuit was used at 50 Hz. The piezoelectric charge constant (d_{33}) was measured after poling by the piezometer (Take Control, PM 35).

3. Results and discussion

3.1. XRD analysis

The XRD patterns of pure and La-modified PZTFN are depicted in Fig. 1. All of the specimens exhibit the single-phase formation in powders with the exception of the x = 0.016 sample, in which case a small amount of secondary phase is present in the composition. For a tetragonal (T) phase, the (200) reflection is a doublet, whereas it is a singlet for a rhombohedral (R) phase. As evident from the XRD patterns, the structure is tetragonal at La concentrations up to x = 0.008. When the La content is further increased to x = 0.012, the peak splitting is clearly observed. However, the nature of peak distortion is not doublet but rather triplet in nature, corresponding to the $(200)_T$, $(200)_R$, and $(002)_T$ peaks [23]. This splitting suggests that the x =

0.012 composition is neither a perfect tetragonal nor a perfect rhombohedral structure but a mixture of both [3]. On the basis of a careful study on the (200) reflections in the XRD patterns, a phase transformation from tetragonal to rhombohedral occurs as a consequence of an increase in the amount of La. The smaller ionic radius of La^{3+} (R = 0.136 nm), compared to that of Pb^{2+} (R = 0.149 nm), promotes the phase transformation from tetragonal to rhombohedral. The MPB can be defined as the coexistence of rhombohedral and tetragonal phases. To confirm the structural parameters of the various compositions accurately, the Rietveld refinements of XRD patterns of the various compositions were conducted using the Fullprof software.

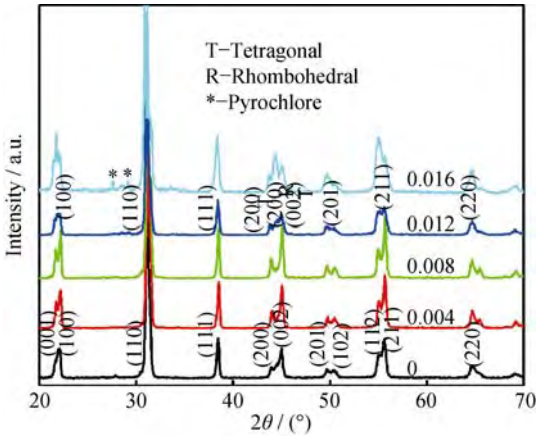

Fig. 1. XRD patterns of La-modified PZTFN ceramics with x = 0, 0.004, 0.008, 0.012, and 0.016.

3.2. Rietveld refinement details

The structure of the polycrystalline sample was refined by the Rietveld method using the Fullprof software [24]. Rietveld refinement was conducted using XRD data in the 2θ range of 20°–70°. The background was fitted with a sixth-order polynomial, and the peak shapes were described by pseudo-Voigt profiles. The complete expression used in the Rietveld method is written as

$$\mathrm{FWHM}^2 = (U + D_{\mathrm{ST}}^2)\tan^2\theta + V\tan\theta + W + \mathrm{IG}/\cos^2\theta \quad (1)$$

where FWHM is the full width at half maximum, U, V, and W the usual peak shape parameters, IG a measure of the isotropic size effect, and D_{ST} the coefficient related to strain. IG and D_{ST} can be refined in the Rietveld method.

During the refinement process, various factors were taken into account, such as the scale factor, zero correction, background, half-width parameters, positional parameters (x, y, z), lattice parameters (a, b, c, α, β, γ), and thermal parameters. The use of anisotropic thermal parameters for Pb and La ions invariability led to an improvement in the Rietveld-refined parameters and was considered in all of the refinements. No correlation was observed in the thermal and positional parameters during the refinement process. Thus, all parameters were refined together. The experimental points were given as red dots and theoretical data were shown as a solid black line. The difference between the theoretical and experimental data was plotted as a green line along the bottom. The vertical line represented the Bragg allowed peak positions.

3.3. Refinement of La-modified PZTFN ceramics

The structure of pure PZT was refined by Ragini *et al.* [3] for different values of x. In their refinement process, they reported that the compositions with $x \leq 0.515$ exhibited a tetragonal structure with space group *P*4*mm*, but in the MPB region, $0.515 < x < 0.53$, the structure was considered as a mixture of tetragonal and monoclinic phases with space groups *P*4*mm* and *Cm*, respectively. Singh *et al.* [25] reported that $(1-x)[Pb(Fe_{1/2}Nb_{1/2})]O_3$–$xPbTiO_3$ (PFN–xPT) contained monoclinic (space group *Cm*) and tetragonal (space group *P*4*mm*) phases near MPB for $0.06 < x < 0.08$. To locate the MPB region in La-modified PZTFN ceramics, various compositions were prepared with $0 \leq x \leq 0.016$. The structure of all the compositions was studied using Rietveld refinements. Typical refined XRD patterns of the La-modified PZTFN ceramics are shown in Fig. 2. The structure-related lattice parameters and goodness-of-fit results are listed in Table 1.

In the tetragonal phase with *P*4*mm* space group, four ions compose the asymmetric unit, with the Pb^{2+}/La^{3+} ion in 1(a) sites at (0, 0, z), $Ti^{4+}/Nb^{5+}/Fe^{3+}$ and O_{I}^{2-} in 1(b) sites at (1/2, 1/2, z), and O_{II}^{2-} in 2(c) sites at (1/2, 0, z). For the rhombohedral phase with *R*3*c* space symmetry, three ions compose the asymmetric unit of the rhombohedral structure, as Pb^{2+}/La^{3+} and $Nb^{5+}/Ti^{4+}/Fe^{3+}$ ions in 3(a) sites at (0, 0, z) and O^{2-} ions in 3(b) sites at (2x, x, 1/6) [25].

Figs. 2(A) (a)–(c) show the Rietveld refinement results based on the tetragonal *P*4*mm* space group, whereas Fig. 2(A) (d) depicts the refined data in consideration of the coexistence of phases with *R*3*c* and *P*4*mm* space symmetry. With an increase in the La content, a structural change occurs in the material, as revealed by the Rietveld refinement results. The tetragonal factor (c/a) decreases with increasing La content because of the decrease in the dipole moment; as a consequence, the transition temperature (T_{c}) is reduced [26].

3.4. Microstructure analysis

Fig. 3 shows the average grain size, bulk density, and

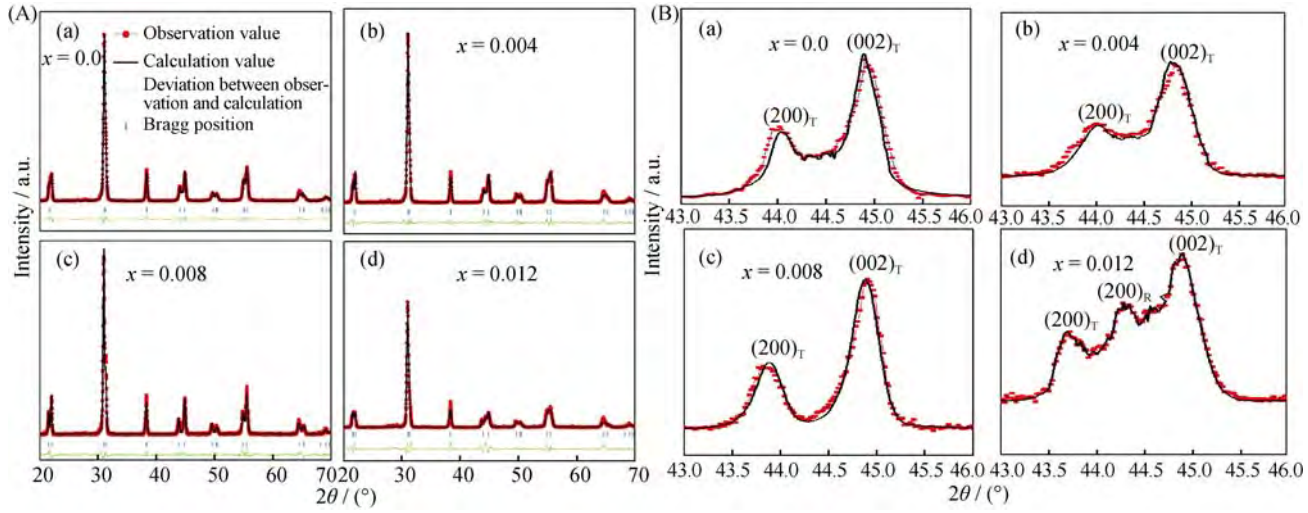

Fig. 2. Rietveld refinement patterns of La-modified PZTFN ceramics at room temperature using space groups *P*4*mm* and *R*3*c* (A) and an expanded refinement of XRD peaks associated with the (200) plane (B).

Table 1. Detail of the Rietveld-refined parameters of the La-modified PZTFN ceramics

Composition	Structure space group	Lattice parameter						Cell volume / nm^3	χ^2	R_p/%	R_{wp}/%	R_{exp}/%	R_{Bragg}	R_F	Mass fraction/%
		a / nm	*b* / nm	*c* / nm	α / (°)	β / (°)	γ / (°)								
x=0	Tetragonal (*P*4*mm*)	0.4043	0.4043	0.4113	90	90	90	0.6725	2.71	1.85	23.1	13.17	4.87	3.41	100
x=0.004	Tetragonal (*P*4*mm*)	0.4047	0.4047	0.4116	90	90	90	0.6744	2.83	18.1	22.1	13.26	4.07	2.52	100
x=0.008	Tetragonal (*P*4*mm*)	0.4048	0.4048	0.4128	90	90	90	0.6750	3.49	18.0	22.0	11.16	6.04	4.21	100
x=0.012	Tetragonal (*P*4*mm*)	0.4048	0.4048	0.4123	90	90	90	0.6858	3.23	25.0	29.0	14.00	8.90	9.25	79.54
	Rhombohedral (*R*3*c*)	0.4025	0.4025	1.29617	90	90	120	1.81927					57.3	37.1	20.46

Note: *a*, *b*, and *c* are the lattice parameters, α, β, and γ the angles between the two intercepts, χ^2 the goodness-of-fit, R_p the profile factor, R_{wp} the weighted profile factor, R_{exp} the expected weight factor, R_{Bragg} the Bragg factor, and R_F the crystallographic factor.

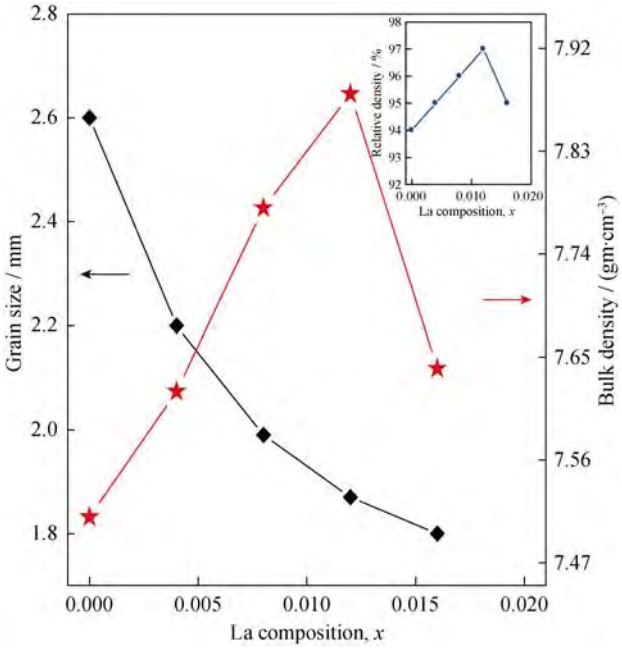

Fig. 3. Variation of the average grain size, bulk density, and relative density as a function of composition.

relative density as a function of La-doped PZTFN ceramics composition. The average grain size was calculated using the line-intercept method. The grain sizes start to decrease with increasing La doping. The average grain size lies between 2.6 and 1.8 μm. Micrographs of all the sintered pellets of the La-modified PZTFN ceramics are presented in Fig. 4. A uniform microstructure is observed in the present study for La-modified PZTFN ceramics. These micrographs suggest that the sintered pellets of La-modified PZTFN are fully dense compared to the undoped PZTFN ceramic, and reveal that the pores are free and the tightly bound grains promote densification in the ceramics. Thus, in the present study, La plays a significant role in defining the microstructural characteristics of PZTFN ceramics and acts as an inhibitor of grain growth. In this system, the homogenization is clearly caused by the greater atomic diffusion.

3.5. Dielectric analysis

Fig. 5 shows the temperature-dependent dielectric behavior for La-modified PZTFN ceramics at 1 kHz. As evi-

dent in the figure, La_2O_3 plays a significant role in governing the phase-transition behavior and dielectric properties of the PZTFN ceramics. In the present study, the transition temperature decreases with increasing La_2O_3 concentration up to $x = 0.008$. However, for $x \geq 0.008$, the transition temperature tends to be almost constant.

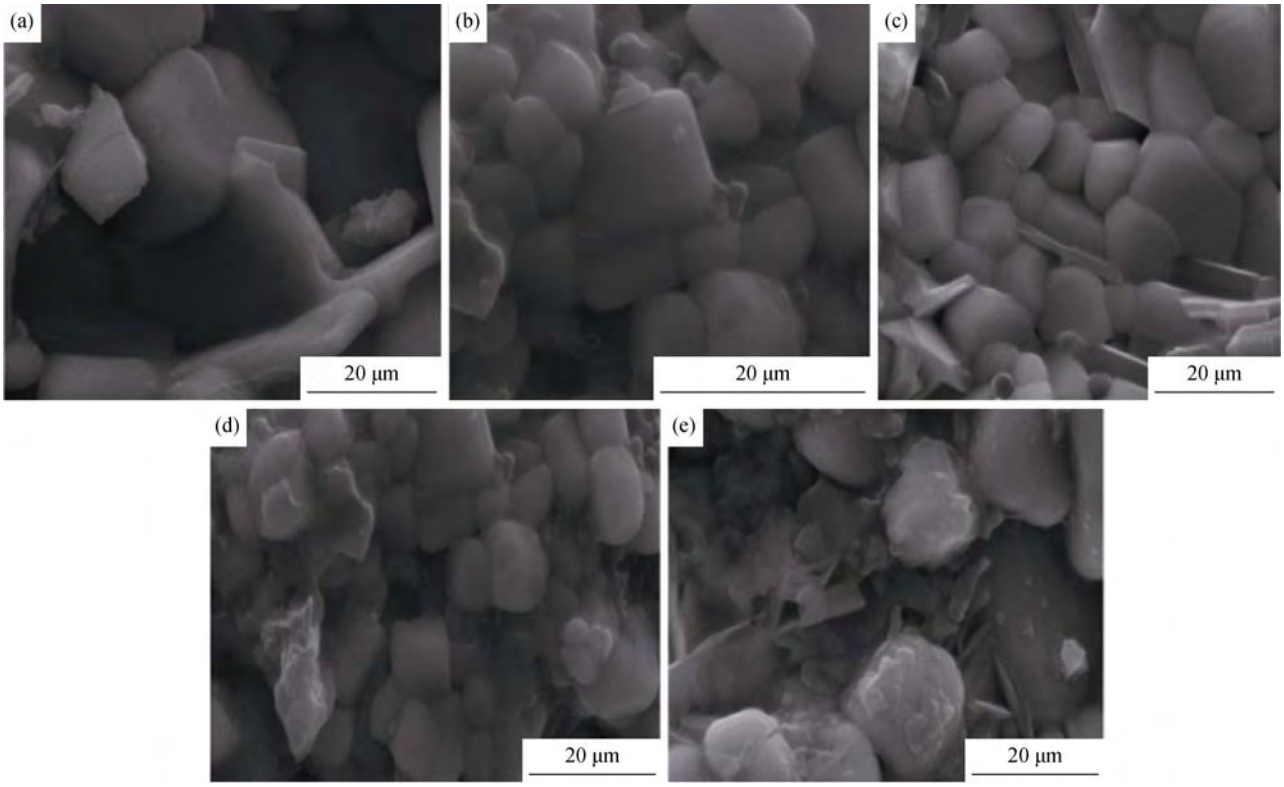

Fig. 4. SEM micrographs of La-modified PZTFN ceramics: (a) $x = 0$; (b) $x = 0.004$; (c) $x = 0.008$; (d) $x = 0.012$; (e) $x = 0.016$.

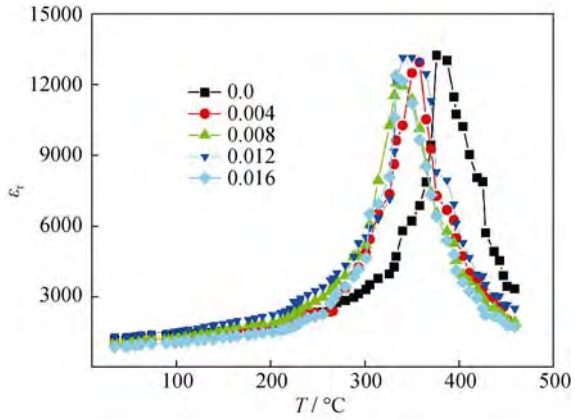

Fig. 5. Temperature-dependent dielectric constants of all the La-modified PZTFN ceramic samples at 1 kHz.

To study the temperature-dependent behavior of dielectric constant (ε_r) and dielectric loss ($\tan\delta$), a comparative measurement of ε_r was conducted at various temperature and different frequencies. Fig. 6 depicts the variation of ε_r and $\tan\delta$ at different frequencies. The dielectric constant decreases with increasing frequency for all compositions. In the case of pure PZTFN, the T_c value is at approximately 376°C. As the La content increases, the T_c value decreases from 376°C to 339°C and its transition temperature broadens. These results, in turn, indicate the typical relaxor ferroelectric behavior caused by the randomly oriented polar microregions that originates from the compositional fluctuations at the nanometer length scale due to La doping [27]. Furthermore, an increase in La content in the A-sites of PZTFN facilitates the domain realignment, which improves the properties of the material.

3.6. Ferroelectric properties

The polarization-electrical field (P–E) hysteresis loops of La-modified PZTFN ceramics at room temperature are depicted in Fig. 7, and the related parameters are listed in Table 2. Well developed and comparatively symmetric hysteresis loops are observed for all of the compositions. As evident in the figure, the ferroelectric properties of PZTFN are influenced by La doping. Furthermore, La doping in PZTFN increases the response of remnant polarization (P_r). The maximum value of remnant polarization (P_{max}) at a

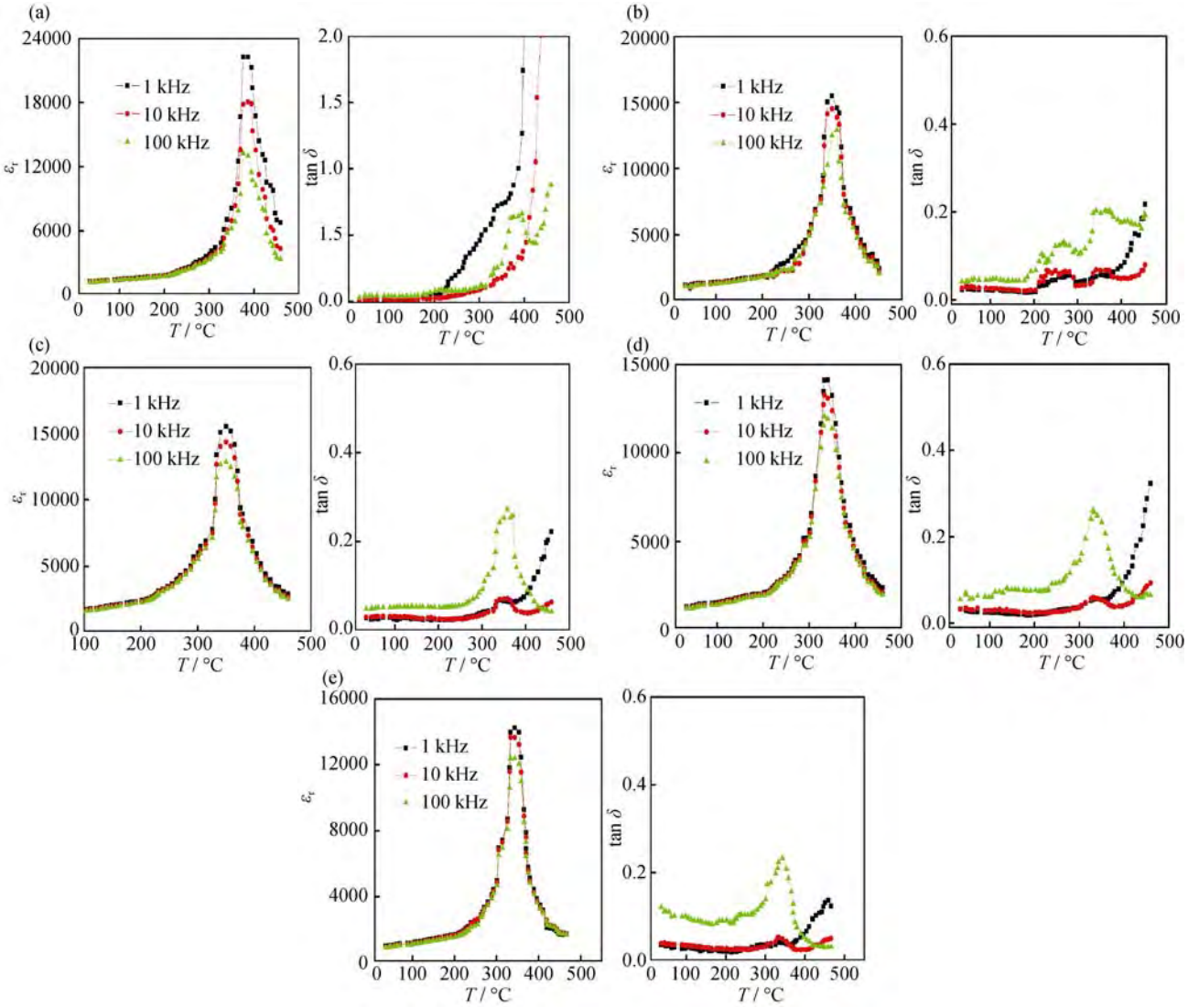

Fig. 6. Temperature-dependent dielectric constants and dielectric losses of La-modified PZTFN ceramics at 1 kHz, 10 kHz, and 100 kHz: (a) x = 0; (b) x = 0.004; (c) x = 0.008; (d) x = 0.012; (e) x = 0.016.

coercive field (E_c) of 12 kV/cm for the composition x = 0.012 is 17.15 μC/cm^2. The remnant polarization increases for La contents up to x = 0.012 and thereafter decreases. The composition x = 0.012, which is close to the MPB region, may contain both tetragonal and rhombohedral phases that coexist to give fourteen possible polarization directions [33]. The enhancement of ferroelectric and piezoelectric properties occurs because of the coexistence of multiple domains [34].

3.7. Piezoelectric properties

Piezoelectric charge coefficients (d_{33}) of undoped and La-modified PZTFN, as measured with a Berlincourt piezometer, are depicted in Fig. 8; the data are summarized in Table 2. In general, the piezoelectric properties increase with the increase of grain size, porosity, and homogeneity, and the change in structure and dopant concentrations. MPB is well known to play a significant role in enhancing the piezoelectric properties of perovskite-structured piezoelectric ceramics, such as PZT [35], $Pb(Mg_{1/3}Nb_{2/3})O_3$–$PbTiO_3$ [28], and $Bi_{0.5}Na_{0.5}TiO_3$–$BaTiO_3$ [36]. With increasing La doping in PZTFN ceramics, the d_{33} value starts to increase sharply up to x = 0.012 and then decreases. The maximum response of d_{33} (368 pC/N) is observed at x = 0.012, which may be attributable to the presence of MPB. With increased La doping at Pb sites, the piezoelectric coefficient reaches a maximum because of the presence of multiple ions in the system [37].

4. Conclusions

La-modified PZTFN ceramics were synthesized via a

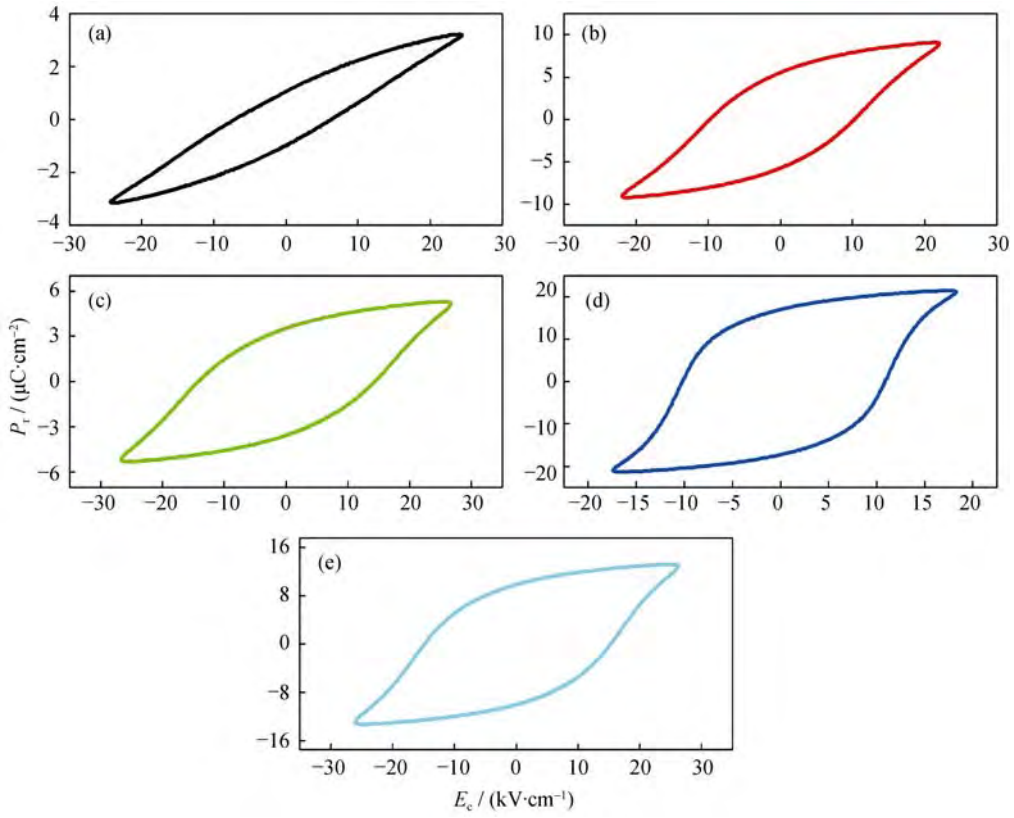

Fig. 7. Hysteresis loops for La-modified PZTFN ceramics at room temperature: (a) x = 0; (b) x = 0.004; (c) x = 0.008; (d) x = 0.012; (e) x = 0.016.

Table 2. Electrical properties of La-modified PZTFN ceramics with values reported in literatures

Composition	ε_r at room temperature	tanδ at room temperature	T_c / ºC	P_r / (μC·cm^{-2})	P_{max} / (μC·cm^{-2})	E_c / (kV·cm^{-1})	d_{33} / (pC·N^{-1})
x=0	1236	0.013	376	1.02	3.03	12.12	270
x=0.004	1288	0.02	350	4.64	8.66	10.56	296
x=0.008	1317	0.026	346	4.55	5.30	14.24	340
x=0.012	1485	0.031	339	17.15	21.46	12.02	368
x=0.016	998	0.035	339	9.90	13.09	16.95	349
Data in references	1000 in Ref. [18], 1100 in Ref. [21], 945 in Ref. [21],	0.013 in Ref. [21], 0.17 in Ref. [28]	385 in Ref. [21], 350 in Ref. [18], 265 in Ref. [29]	18.13 in Ref. [30]	25 in Ref. [30]	—	323 in Ref. [31], 338 in Ref. [32]

semi-wet route. Rietveld analysis of XRD patterns reveals that the samples with the composition of $x \leq 0.08$ have a tetragonal structure with *P*4*mm* space symmetry. The coexistence of tetragonal (space group *P*4*mm*) and rhombohedral (space group *R*3*c*) phases occurs at $x \geq 0.012$, which corresponds to the morphotropic phase boundary (MPB) of PLZTFN ceramics. Microstructures of all the samples reveal that the average grain size is reduced with the increase in La doping. The dielectric, ferroelectric, and piezoelectric properties of the La-modified PLZTFN ceramics are significantly improved near the MPB. The values of piezoelectric coefficient (d_{33}), dielectric constant (ε_r), dielectric loss (tanδ), remnant polarization (P_r), and coercive field (E_c) for the composition of x = 0.012 are 368 pC/N, 1485, 0.03, 17.15 μC/cm^2, and 12.02 kV/cm, respectively. The PLZTFN ceramics near MPB exhibit the improved *P*–*E* square loops compared to those for pure PZT, which can be utilized for the better performance in random access memory applications.

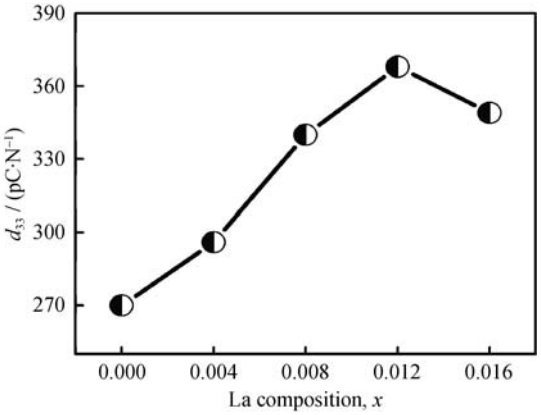

Fig. 8. Variation of piezoelectric charge coefficients (d_{33}) with La composition (x).

Acknowledgements

This work was financially supported by the Defence Research and Development Organisation (DRDO), the Government of India (No. ERIP/ER/0903830/M/01/1235).

References

[1] N. Setter, Electroceramics: looking ahead, *J. Eur. Ceram. Soc.*, 21(2001), p. 1279.

[2] R.C. Buchanan, *Ceramic Materials for Electronics*: *Processing Properties, and Applications*, Marcel Dekker Inc., New York, 1986, p. 139.

[3] Ragini, R. Ranjan, S.K. Mishra, and D. Pandey, Room temperature structure of $Pb(Zr_xTi_{1-x})O_3$ around the morphotropic phase boundary region: a Rietveld study, *J. Appl. Phys.*, 92(2002), No. 6, p. 3266.

[4] B.V. Hiremath, A.I. Kingon, and J.V. Biggers, Reaction sequence in the formation of lead zirconate-lead titanate solid solutions: role of raw materials, *J. Am. Ceram. Soc*., 66(1983), No. 11, p. 790.

[5] A. Dalakoti, A. Bandyopadhyay, and S. Bose, Effect of Zn, Sr, and Y addition on electrical properties of PZT thin films, *J. Am. Ceram. Soc*., 89(2006), No. 3, p. 1140.

[6] B.W. Lee and E.J. Lee, Effects of complex doping on microstructural and electrical properties of PZT ceramics, *J. Electroceram.*, 17(2006), p. 597.

[7] M. Prabu, I.B.S. Banu, S. Gobalakrishnan, and M. Chavali, Electrical and ferroelectric properties of undoped and La-doped PZT (52/48) electroceramics synthesized by sol–gel method, *J. Alloys Compd.*, 551(2013), p. 200.

[8] K. Ramam and M. Lopez, Ferroelectric and piezoelectric properties of Ba modified lead zirconium titanate ceramics, *J. Phys. D*, 39(2006), p. 4466.

[9] D. Bochenek, Properties of the ferroelectric PBZT ceramics admixed with niobium, *Ferroelectrics*, 417(2011), p. 41.

[10] A. Singh and R. Chatterjee, Multiferroic properties of La-Rich $BiFeO_3$–$PbTiO_3$ solid solutions, *Ferroelectrics*, 433(2012), p. 180.

[11] Brajesh K, A.K. Himanshu, H. Sharma, K. Kumari, R. Ranjan, S.K. Bandhopadhyay, and T.P. Sinha, Structural, dielectric relaxation and piezoelectric characterization of Sr^{2+} substituted modified PMS-PZT ceramic, *Phys B*, 407(2012), p. 635.

[12] A. Kumar and S.K. Mishra, Effects of Sr^{2+} substitution on the structural, dielectric, and piezoelectric properties of PZT-PMN ceramics, *Int. J. Miner. Metall. Mater*., 21(2014), p. 175.

[13] J. Ryu, J.J. Choi, and H.E. Kim, Effect of heating rate on the sintering behavior and the piezoelectric properties of lead zirconate titanate ceramics, *J. Am. Ceram. Soc.*, 84(2001), No. 4, p. 902.

[14] S. Dutta and R.N.P. Choudhary, Synthesis and characterization of Fe^{3+} modified PLZT ferroelectrics, *J. Mater. Sci. Mater. Electron.*, 14(2003), p. 463.

[15] S.Y. Chu, T.Y. Chen, I.T. Tsai, and W. Water, Doping effects of Nb additives on the piezoelectric and dielectric properties of PZT ceramics and its application on SAW devices, *Sens. Actuators A*, 113(2004), p. 198.

[16] V.Y. Toplov, Heterophase structures and their quantitative characteristics in $(1-x)Pb(Fe_{1/2}Nb_{1/2})O_3$–$xPbTiO_3$ near the morphotropic phase boundary, *Mater. Lett*., 66(2012), p. 57.

[17] F. Kahoul, L. Hamzioui, N. Abdessalem, and A. Boutarfaia, Synthesis and piezoelectric properties of $Pb_{0.98}Sm_{0.02}[(Zr_y, Ti_{1-y})_{0.98}(Fe^{3+}_{1/2}, Nb^{5+}_{1/2})_{0.02}]O_3$ ceramics, *Mater. Sci. Appl.*, 3(2012), p. 50.

[18] A. Prasatkhetragarn, Synthesis and dielectric properties of $0.9Pb(Zr_{1/2}Ti_{1/2})O_3$–$0.1Pb(Fe_{1/3}Nb_{2/3})O_3$ ceramics, *Ferroelectrics*, 416(2011), p. 35.

[19] R. Rai, S. Sharma, and R.N.P. Choudhary, Dielectric and piezoelectric studies of Fe doped PLZT ceramics, *Mater. Lett*., 59(2005), p. 3921.

[20] A.K. Shukla, V.K. Agrawal, I.M. Das, J. Singh, and S.L. Srivastava, Dielectric response of PLZT ceramics *x*/57/43 across ferroelectric-paraelectric phase transition, *Bull. Mater. Sci.*, 34(2011), p. 133.

[21] F. Kahoul, L. Hamzioui, Z. Necira, and A. Boutarfaia, Effect of sintering temperature on the electromechanical properties of $(1-x)Pb(Zr_yTi_{1-y})O_3$–$xSm(Fe^{3+}_{0.5}, Nb^{5+}_{0.5})O_3$ ceramics, *Energy Procedia*, 36(2013), p. 1050.

[22] A.P. Singh, S.K. Mishra, D. Pandey, C.D. Prasad, and R. Lal, Low temperature synthesis of chemically homogeneous lead zirconate titanate (PZT) powder by a semi-wet method, *J. Mater. Sci.*, 28(1993), No. 18, p. 5050.

[23] M.R. Soares, A.M.R. Senos, and P.Q. Mantas, Phase coexistence region and dielectric properties of PZT ceramics, *J. Eur. Ceram. Soc.*, 20(2000), p. 321.

[24] J. Rodriguez-Carvajal, Recent advances in magnetic structure determination by neutron powder diffraction, *Phys. B*, 192(1993), p. 55.

[25] S.P. Singh, A.K. Singh, and D. Pandey, Evidence for a monoclinic M_A to tetragonal morphotropic phase transition in

$(1-x)[Pb(Fe_{1/2}Nb_{1/2})O_3]-xPbTiO_3$ ceramics, *J. Phys. Condens. Matter*, 19(2007), art. No. 036217.

[26] D.M. Santos, A.Z. Simoes, M.A. Zaghete, C.O.P. Santos, J.A. Varela, and E. Longo, Synthesis and electrical characterization of tungsten doped $Pb(Zr_{0.53}Ti_{0.47})O_3$ ceramics obtained from a hybrid process, *Mater. Chem. Phys.*, 103(2007), p. 371.

[27] S.B. Krupanidhi, Relaxor type perovskites: primary candidates of nano-polar regions, *J. Chem. Sci*., 115(2003), p. 775.

[28] B. Noheda, D.E. Cox, G. Shirane, J. Gao, and Z.G. Ye, Phase diagram of the ferroelectric relaxor $(1-x)PbMg_{1/3}Nb_{2/3}O_3-x$-$PbTiO_3$, *Phys. Rev. B*, 66(2002), art. No. 054104.

[29] L. Kozielski and F. Clemens, Multiferroics application: magnetic controlled piezoelectric transformer, *Process. Appl. Ceram.*, 6(2012), p. 15.

[30] B. Sahoo and P.K. Panda, Effect of lanthanum, neodymium on piezoelectric, dielectric and ferroelectric properties of PZT, *J. Adv. Ceram*., 2(2013), p. 37.

[31] A.K. Zak, A. Jalalian, S.M. Hossseini, A. Kompany, and T.S. Narm, Effect of Y^{3+} and Nb^{5+} co-doping on dielectric and piezoelectric properties of PZT ceramics, *Mater. Sci.*, 28(2010), p. 703.

[32] V. Singh, H.H. Kumar, D.K. Kharat, S. Haits, and M.P. Kulkarni, Effect of lanthanum substitution on ferroelectric properties of niobium doped PZT ceramics, *Mater. Lett*., 60(2006), p. 2964.

[33] C.A. Randall, N. Kim, J.P. Kucera, W.W. Cao, and T.R. Shrout, Intrinsic and extrinsic size effects in fine grained morphotropic phase boundary lead zirconate titanate ceramics, *J. Am. Ceram. Soc*., 81(1998), p. 677.

[34] Z.H. Yao, H.X. Liu, Y.Q. Li, M.H. Cao, and H. Hao, Morphotropic phase boundary of $(Bi_{0.9}La_{0.1})ScO_3$–$PbTiO_3$ piezoelectric ceramics for high-temperature application, *Ferroelectrics*, 409(2010), p. 21.

[35] B. Noheda, D.E. Cox, G. Shirane, R. Guo, B. Jones, and L.E. Cross, Stability of the monoclinic phase in the ferroelectric perovskite $PbZr_{1-x}Ti_xO_3$, *Phys. Rev. B*, 63(2001), art. No. 014103.

[36] T. Takenaka, K. Maruyama, and K. Sakata, $(Bi_{1/2}Na_{1/2})TiO_3$–$BaTiO_3$ system for lead-free piezoelectric ceramics, *Jpn. J. Appl. Phys*., 30(1991), p. 2236.

[37] B.M. Jin, D.S. Lee, I.W. Kim, J.H. Kwon, K.S. Lee, J.S. Song, and S.J. Jeong, The additives for improving piezoelectric and ferroelectric properties of $0.2Pb(Mg_{1/3}Nb_{2/3})O_3$–$0.8(PbZrO_3–PbTiO_3)$ ceramics, *Ceram. Int*., 30(2004), p. 1449.